Journal of Materials Chemistry A

Membrane-modified Electrocatalysts for Nitrate Reduction to Ammonia with High Faradaic Efficiency

Journal:	*Journal of Materials Chemistry A*
Manuscript ID	TA-ART-09-2022-006938.R1
Article Type:	Paper
Date Submitted by the Author:	06-Oct-2022
Complete List of Authors:	Mondol, Profulla; University of Nevada, Reno, Department of Chemistry Panthi, Dipak; University of Nevada, Reno, Department of Chemistry Albarran Ayala, Adan; University of Nevada, Reno, Department of Chemistry Odoh, Samuel; University of Nevada, Reno, Department of Chemistry Barile, Christopher; University of Nevada, Reno, Department of Chemistry

Membrane-modified Electrocatalysts for Nitrate Reduction to Ammonia with High Faradaic Efficiency

Profulla Mondol, Dipak Panthi, Adan J. Albarran Ayala,

Samuel O. Odoh, and Christopher J. Barile*

Department of Chemistry, University of Nevada, Reno, Reno, NV 89557, USA

*E-mail: cbarile@unr.edu

Abstract

In light of the enormous energy footprint of the Haber-Bosch process (1-2% of global energy consumption), alternative green routes of generating ammonia (NH_3) are needed. The electrochemical reduction of NO_3^- from waste streams is a promising method to produce NH_3 using renewably-sourced electricity. However, catalyst selectivity is a grand challenge that hinders NO_3^- to NH_3 conversion technologies. In this manuscript, we fabricate Nafion-modified metal catalysts for NO_3^- reduction. Although Nafion composites are commonly used to facilitate proton transfer, this work investigates electrodes covered by Nafion overlayers, which possess unique reactivity. We find that Cu versions of these catalysts reduce NO_3^- to NH_3 with a Faradaic efficiency of up to (91 ± 2) %, making them among the most selective catalysts reported. Voltammetry studies, surface-enhanced Raman spectroscopy, and density functional theory calculations indicate that the Nafion overlayer activates the N-O bond of a key Cu-NO intermediate, thus facilitating NH_3 production. Lastly, we demonstrate that these catalysts are effective at denitrifying polluted groundwater samples in the field.

Keywords: nitrate reduction, electrocatalysis, membrane-modified catalysis, NO activation

Introduction

Ammonia (NH_3) is an extremely important chemical feedstock and is used extensively in the fertilizer, pharmaceutical, and dye industries.[1-4] As a result, NH_3 is the fifth most produced chemical in the world by volume.[5] Additionally, NH_3 has recently been considered as an alternative renewable fuel in fuel cells.[6,7] The most well-established route to generate NH_3 on an industrial scale is the Haber-Bosch process.[6,8-11] Because the Haber-Bosch process is energy intensive and because a massive quantity of NH_3 is generated annually, NH_3 production is responsible for 1-2% of total world energy consumption and causes ~1% of global anthropogenic CO_2 emissions.[2,12-14] Another route to produce NH_3 is through the electrochemical generation of H_2 from water coupled with subsequent N_2 reduction.[1] However, there are several large challenges associated with electrochemical N_2 reduction including low selectivity, low current densities, low N_2 solubility in water, and the high dissociation energy of the N≡N bond, all of which have prevented the use of electrochemical N_2 reduction to NH_3 outside of research settings.[13,15]

Alternatively, NH_3 can be produced electrochemically from the nitrate anion (NO_3^-). In many respects, NO_3^- is a better source of nitrogen because of its high water solubility and the low dissociation energy of the N=O bond compared to N≡N, which allows for faster reaction kinetics.[16] Another value of using NO_3^- is its high natural abundance, [17,18] particularly in agricultural settings where it is a major environmental pollutant. Thus, the electrochemical generation of NH_3 from NO_3^- under ambient conditions has the potential not only to save energy consumption vis-à-vis the Haber-Bosch process, but it could also play an important role in environmental remediation. For example, high concentrations of NO_3^- in drinking water cause several health problems including blue baby syndrome, thyroid disease, birth defects, and cancer.[19] For this reason, the United States Environmental Protection Agency (EPA) has set a limit of 10 mg/L of NO_3^- in drinking water. [20,21]

In contrast, NH_3 is comparatively less toxic, and the EPA has not established a threshold for NH_3 concentration in drinking water.

Previous research has demonstrated the activity of monometallic catalysts such as Pd,[22] Pt,[22] Ag,[23] Cu,[23] Sn,[24] and Rh for NO_3^- and/or nitrite (NO_2^-) reduction.[23] Bimetallic catalysts including Pt-Cu,[22,25] Pd-Cu,[22] Pd-Sn,[26] Sn-Rh,[27] Sn-Ru,[27] and Sn-Ir[27] have also been used. Nonetheless, selectivity remains a challenge, and for NO_3^- to NH_3 catalysts, N_2 and H_2 are common side products that diminish NH_3 Faradaic efficiency.[28]

Electrocatalyst selectivity is a concern for all reactions involving multiple proton and electron transfer steps and is not just limited to the NO_3^- reduction reaction. For example, our group designed new membrane-modified catalysts that can be used to increase the selectivity of the CO_2 reduction reaction.[29,30] In particular, we demonstrated that when the fluoropolymer Nafion is used as an overlayer that interfaces the catalyst and bulk solution, a bound CO intermediate is activated on the catalyst surface.[30] This activation of CO allows it to be further reduced to CH_4, the most highly reduced form of carbon.

Based on these previous results, we hypothesize that a similar strategy can be used to increase the selectivity of NO_3^- to NH_3 catalysts. In NO_3^- reduction, NH_3 is the most reduced product, making it the direct analog of CH_4 in CO_2 reduction. Furthermore, the electronic and structural properties of NO and CO are similar, and NO is a key intermediate in the NO_3^- reduction reaction just as CO is an important intermediate in CO_2 reduction.[31-34] For these reasons, we speculate that a metal-NO intermediate could be activated by a Nafion overlayer to increase the selectivity of NH_3 production. This manuscript provides experimental and computational evidence in support of this central hypothesis.

Nafion is a widely used fluoropolymer that is often mixed with electrocatalysts to facilitate proton transport or used as a separator between two half reaction compartments in full NO_3^- reduction devices.[35,36] In contrast to these uses of Nafion, this work studies different metallic electrodes covered by Nafion overlayers. In this architecture, Nafion affects the reactivity of intermediates at the catalyst surface, and thus its role here is fundamentally different from the other common uses of fluoropolymers in electrocatalyst research.

Experimental procedures

Materials and Electrode Preparation

Nafion D520 dispersion was purchased from Fuel Cell Store, Inc. Cu foil (99.99%) was purchased from All-Foils, Inc. Ti foil (99.99%) was purchased from Stanford Advanced Materials, Pb foil was purchased from KRT Distributions (99.9%), and Zn foil (99.99%) was purchased from Belmont Metals. $NaNO_3$ (> 99%) and Na_2SO_4 (> 99%) were purchased from Sigma Aldrich. $NaNO_2$ (98%) was purchased from Oakwood Chemicals, Inc. The pH of solutions was measured using a Go Direct pH sensor (Vernier, Inc.). The unadjusted pH of the electrolytes was approximately 5.5 due to the presence of atmospheric CO_2 in the water. More acidic electrolytes were pH adjusted with sulfuric acid. Nafion-modified electrodes were fabricated by drop-casting the Nafion dispersion directly onto the metal surfaces. To modify the thickness of the Nafion layer, multiple rounds of drop-casting were performed. In between each round of drop-casting, the Nafion dispersion was dried in an oven for 7 min at 65 °C.

Electrochemical Measurements

A VSP-300 Biologic potentiostat was used for electrochemical studies. All electrochemical studies were performed in a three-electrode system in which metal surfaces, a platinized-titanium

electrode (Rio Grande, Inc.), and a leakless Ag/AgCl/3 M KCl (eDaq, Inc.) were the working, counter, and reference electrodes, respectively. Current densities are reported with respect to the geometric area of the working electrode. The metal electrodes were rinsed with acetone and subsequently washed with deionized water several times before use. For evaluating NO_3^- reduction activities of each thin film, the working electrodes were studied in 10 mL of 50 mM $NaNO_3$ and 100 mM Na_2SO_4 (unless otherwise mentioned) in a two-compartment cell. The cell consisted of a 25 mL glass beaker separated by a Nafion 117 membrane (H^+ form, 183 μm, Fuel Cell Store, Inc.). The working and reference electrodes were in one compartment, while the counter electrode was placed in the second compartment. The onset potential was determined by calculating the potential at which the current density reached 10% of the maximum current density for each LSV.

For electrochemical NO_2^- reduction, we used 10 mL 50 mM $NaNO_2$ and 100 mM Na_2SO_4 in a two-compartment electrochemical cell and followed a procedure analogous to those used for NO_3^-. For electrochemical NO reduction, we used 10 mL 100 mM Na_2SO_4. This electrolyte was sparged with NO gas for 10 minutes before running chronoamperometry. NO was synthesized from $NaNO_2$ and dilute sulfuric acid according to literature procedures.[37] The concentration of NO in a saturated aqueous solution is about 2 mM.[38] For experiments with groundwater, water was obtained from a domestic well in Silver Springs, NV and was used directly in experiments without any pretreatment step.

Materials Characterization

Scanning electron microscope (SEM) images and energy-dispersive X-ray (EDX) analysis were obtained for each sample using a JEOL JSM-7100F field emission SEM operated using an accelerating voltage of 15 kV. X-ray diffraction (XRD) spectra were recorded using a Bruker D2 X-ray diffractometer. A Renishaw in Via confocal Raman microscope was used to collect Raman

spectra of the electrodes. For surface-enhanced Raman spectroscopy experiments with NO gas, NO was sparged for 10 minutes on the Cu surface before collecting the spectra. The Nafion-modified Cu substrates had a thickness of about 100 nm. Although we also collected spectra on Cu with the micron-thick Nafion overlayers used for electrochemical experiments, these spectra only possessed Nafion peaks and could not be used to probe the Cu-Nafion interface due to their large thicknesses. Before all of the experiments, the instrument was calibrated with a Si standard. Spectra were collected with a 10x objective lens and averaged over 10 scans. A 514 nm laser with a power of approximately 11 mW was used to illuminate the samples.

Product Detection

The concentration of NH_3, NO_2^-, and NO_3^- after 1 hour of chronoamperometry were each evaluated using well-established colorimetric methods. For most electrodes, the voltage values used during chronoamperometry were selected such that the current density was approximately 5 mA cm^{-2}. For experiments with Pb electrodes, the current density decreased significantly over the course of 1 hr, and so a high voltage of -2.0 V was used in accordance with previous literature methods.[39] NH_3 was qualitatively detected according to a literature method using iodine.[40] After chronoamperometry, 1 mL of the electrolyte adjusted to pH 13 with 10 wt. % NaOH was poured onto a 3 mg iodine crystal in a small glass vial. A black precipitate of NH_4I_3 upon stirring confirms the presence of NH_3 in the electrolyte. The amount of NH_3 was quantified from the electrolyte using the indophenol method.[41] All the reagents were purchased from Sigma Aldrich and were used without any further purification. 0.5 mL of the catholyte was taken in a glass vial, and 2 mL of a 1 M NaOH solution containing 5 wt. % salicylic acid and 5 wt. % sodium citrate was added. Then, 1 mL of 0.5 M NaClO and 0.2 mL of 1 wt. % sodium nitroferricyanide were added to the same vial. After waiting for 1 hr at room temperature, UV-Vis spectroscopy was performed

(Shimadzu UV-2550 spectrometer). The concentration of NH_3 in the electrolyte was determined using the maximum absorbance at 670 nm along with an appropriate calibration curve produced using NH_3 solutions of known concentrations.

NO_3^- and NO_2^- were evaluated using Griess reagents with and without VCl_3.[42] N-(1-Naphthyl)ethylenediamine dihydrochloride (NEDD) and sulfanilamide were purchased from Sigma Aldrich. A 200 mL 0.5 M sulfuric acid solution containing 2 wt. % NEDD and 2 wt. % sulfanilamide was first prepared to make the Griess reagents.

To quantify NO_2^-, 10 μL of reaction electrolyte was diluted with 2 mL of deionized water, and 0.8 mL of the Griess reagents were added. The solution was let to stand at room temperature for 30 minutes. The absorbances of the resulting solutions were measured using UV-VIS spectroscopy. The concentration of NO_2^- was calculated from the absorbance at 540 nm along with an appropriate calibration curve using NO_2^- solutions of known concentrations.

To detect the amount of NO_3^- consumed during electrochemistry, we used a similar procedure as for NO_2^- detection, except the 200 mL Griess reagent solution contained 0.5 g VCl_3 (Sigma Aldrich). NO_3^- is reduced into NO_2^- by VCl_3 through a relatively slow process, so the reaction was allowed to go to completion by letting the reaction mixture stand at room temperature for 6-10 hours. Finally, the amount of NO_3^- was subtracted from NO_2^- to determine the amount of NO_3^- remaining after electrochemistry.

Faradaic Efficiency Calculations

To calculate the Faradic efficiency (% FE) of NH_3 and NO_2^- production, we used the following formula.

$$\% \text{ FE} = \frac{Actual\ Yield}{Theoritical\ Yield} \times 100 \qquad \ldots\ldots\ldots\ldots\ldots\ldots (1)$$

The Faradic efficiencies of N_2 and H_2 production were calculated from equations considering the feasible NO_3^- reduction products, which are as follows.

$2H^+ + 2e^- \rightarrow H_2$ …….. (2)

$9H^+ + NO_3^- + 8e^- \rightarrow NH_3 + 3H_2O$ ……..…… (3)

$12H^+ + 2NO_3^- + 10e^- \rightarrow N_2 + 6H_2O$ ……..……. (4)

$2H^+ + NO_3^- + 2e^- \rightarrow NO_2^- + H_2O$ ……..… (5)

The catalysts studied in this work did not produce any measurable quantities (Faradaic efficiency > 0.1%) of NO, N_2O, or N_2H_4. NO and N_2O were detected using an Agilent Technologies GC-MS instrument equipped with a 7890A GC system and 5975C inert MSD with a Triple-Axis Detector. N_2H_4 was detected using the para-dimethylaminobenzaldehyde method.[43] In the absence of NO, N_2O, and N_2H_4 production, the number of moles of N_2 can be quantified by determining the amount of NO_3^- consumed (Equation 7). The Faradaic efficiency of N_2 was then calculated from Equation (1).

$n_{NO_3^-}$ (initial) = $n_{NO_3^-}$ (final) + $n_{NO_3^-}$ (consumed)

$n_{NO_3^-}$ (consumed) = $n_{NH_3} + 2n_{N_2} + n_{NO_2^-}$ …… (6)

$n_{N_2} = 0.5\ n_{NO_3^-}$ (consumed) $- 0.5\ n_{NH_3} - 0.5\ n_{NO_2^-}$ ……. (7)

H_2 production was calculated by subtracting the total Faradaic efficiency for nitrogen-containing products from 100%. The values obtained from H_2 production were also corroborated by pH measurements conducted on both compartments of the cell because the number of protons transferred for each nitrogen-containing product is known.

DFT Calculations

All calculations were performed with the PBE-D3 density functional in the Quantum Espresso package. We used large cells and were thus able to sample the Brillouin zone only at the Γ-point. Specifically, we used a 4 * 4 cell with three layers. Scalar-relativistic Projector Augmented Wave (PAW) pseudopotentials were employed with kinetic and charge cut-offs of 50.0 Ry and 420.0 Ry, respectively, while converging all energies to a 10^{-7} Ry threshold.

Results and Discussion

Electrocatalytic NO_3^- Reduction

SEM-EDX analysis demonstrates the successful fabrication of metal electrodes with uniform layers of Nafion with thicknesses ranging from 3-10 μm using a simple dropcasting method (Figures S1 and S2). Electrochemical impedance spectroscopy was subsequently performed on unmodified Cu and Nafion-modified Cu electrodes (Figure S3). The total calculated resistance of the Nafion-modified Cu is higher than the unmodified electrode, which is expected due to the addition of the resistive Nafion layer. We proceeded to evaluate the electrochemical activity of these electrodes for NO_3^- reduction using linear sweep voltammetry (LSV) with and without NO_3^- or NO_2^- in the electrolyte. On an unmodified Cu electrode, the cathodic current increases as the voltage is swept negative in a NO_3^- electrolyte (Figure 1A, black line). The onset potential of electrocatalytic reduction, defined as the potential at which the current reaches 10% of its maximum value during the LSV, is -0.93 V vs. Ag/AgCl. The same unmodified Cu electrode in a NO_2^- electrolyte (Figure 1A, red line) exhibits a similar amount of current as the NO_3^- curve with a slightly more positive onset potential of -0.92 V. These results match previous literature showing that the ability of Cu to reduce NO_2^- at a more positive potential than NO_3^- indicates that Cu is a more effective NO_3^- reduction catalyst than most other metals.[44] A LSV without NO_3^- or NO_2^- containing solely the Na_2SO_4 supporting electrolyte catalyzes the H_2 evolution reaction at a much more negative onset potential of -1.42 V. Polycrystalline Cu is used as a substrate in this

work, and the XRD spectrum of the Cu is displayed in Figure S4, which shows that the (220) face is the most intense peak. Previous experiments with single crystal Cu electrodes demonstrate that the electrocatalytic properties of NO_3^- reduction vary depending upon the crystal face used.[45]

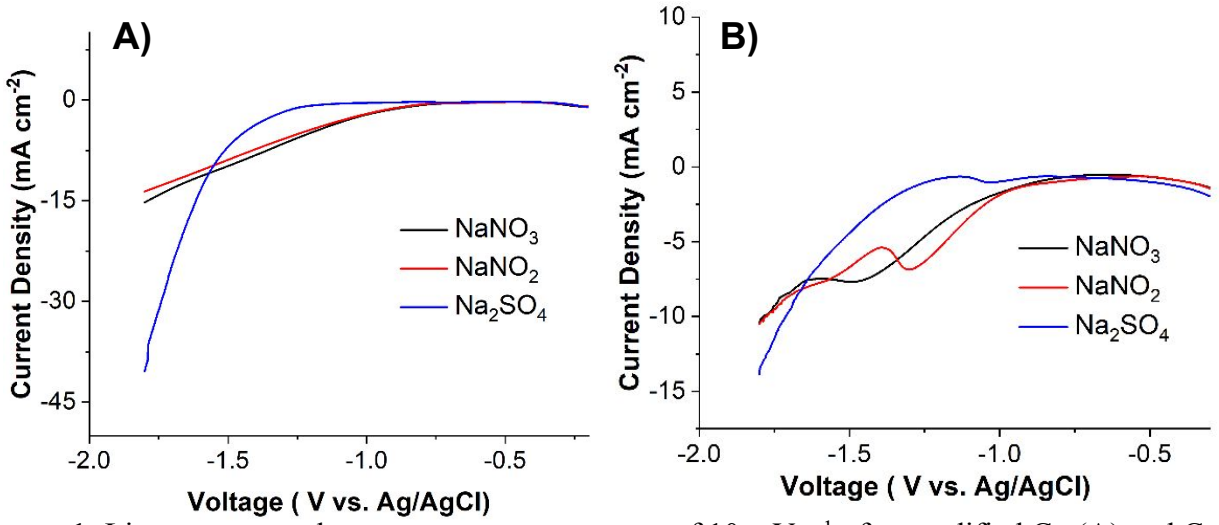

Figure 1: Linear sweep voltammograms at a scan rate of 10 mV s^{-1} of unmodified Cu (A) and Cu modified with 6 μm of Nafion (B) in 50 mM $NaNO_3$ and 100 mM Na_2SO_4 (black line), 50 mM $NaNO_2$ and 100 mM Na_2SO_4 (red line), and 100 mM Na_2SO_4 (blue line).

LSVs in the same three electrolytes with Cu electrodes modified with 6 μm of Nafion (Figure 1B) differ in two important ways from LSVs of unmodified Cu. Firstly, the current densities of the LSVs decrease upon addition of Nafion. This result is expected because the Nafion membrane slows down mass transport from the bulk solution to the electrode. Secondly, and more interestingly, the onset potentials for both NO_3^- (-0.88 V) and NO_2^- (-0.86 V) reduction shift to more positive values in the presence of the Nafion overlayer. This finding indicates that NO_3^- reduction is more thermodynamically favorable with the Nafion. Furthermore, the onset potential for NO_3^- reduction consistently shifts to more positive values as the thickness of the Nafion membrane increases from 3 μm to 10 μm (Figure S5). As with the unmodified electrode, the Nafion-modified electrode still exhibits a slightly more positive onset potential for NO_2^- compared

to NO_3^-, which indicates that the unique NO_3^- reactivity on Cu discussed in the previous paragraph is maintained in the presence of Nafion.

Given the increase in thermodynamic feasibility of NO_3^- reduction with the Nafion-modified Cu electrode, we wondered if the acidic nature of the sulfonate groups of Nafion altered the reactivity of the electrode through a pH effect. To explore this hypothesis, we conducted LSVs in pH 1 electrolytes on unmodified Cu electrodes (Figure S6). Although the onset potential of the LSV (-0.65 V) in the pH-adjusted NO_3^- electrolyte (pH 1) shifts positive compared to the unaltered NO_3^- electrolyte (pH 5.5), the current density for the pH 1 electrolyte in the absence of NO_3^- (Figure S6, blue line) is more than double that of the LSV in the presence of NO_3^- at pH 1 (Figure S6, black line) at most potentials. This dramatic increase in current density in the absence of NO_3^-, which does not occur with the Nafion-modified electrodes (Figure 1B, blue line), suggests that the H_2 evolution reaction is accelerated at pH 1. Indeed, product detection analysis at both pH 1 and 3 demonstrates that the yield of H_2 is significantly higher for these unmodified electrodes (Figure S7) as compared to the Nafion-modified electrode (*vide infra*). In summary, the differences in both the LSVs and product distributions between the Nafion-modified Cu electrode at pH 5.5 and the unmodified Cu electrode under more acidic conditions indicate that the changes in the electrochemical behavior upon addition of the Nafion layer cannot be fully rationalized by pH changes at the electrode-electrolyte interface. Systemic electrochemical analysis, Raman spectroscopy, and density functional theory (DFT) calculations presented later in this manuscript suggest that it is the activation of a Cu-NO intermediate by Nafion that is responsible for the positive shift in the onset potential for NO_3^- reduction on Nafion-modified Cu electrodes.

We next evaluated the NO_3^- product distribution for unmodified and Nafion-modified metal electrodes (Figure 2A). After one hour of chronoamperometry, analytical techniques were

used to assess for a wide variety of nitrogen-containing reduction products including NH_3, NO_2^-, N_2, N_2H_4, NO, and N_2O. None of the electrodes studied produced any detectable quantities (Faradaic efficiencies > 0.1%) of N_2H_4, NO, and N_2O. With the exception of the unmodified Pb electrode which yielded (16 ± 2) % N_2, all electrodes generated NH_3 and NO_2^- as the only nitrogen-containing products. For the unmodified metal electrodes studied, these results are in agreement with previous literature reports.[39] Because NH_3 and NO_2^- are the only nitrogen-containing products, H_2, a common side product in NO_3^- reduction experiments, is assumed to be the remaining product.[46]

At -1.4 V vs. Ag/AgCl, the Cu electrode modified with 6 μm of Nafion produces a strikingly high yield of NH_3, (91 ± 2) %, a value that is higher than the (62 ± 2) % NH_3 Faradaic efficiency for unmodified Cu. Systematic variations in the thickness of Nafion used and the applied voltage show that the highest yield of NH_3, (91 ± 2) %, is obtained with 6 μm of Nafion at -1.4 V (Figures S8-S10). This NH_3 yield with the Cu electrode with 6 μm of Nafion is among the highest reported across all previous literature reports (Table S1). Compared to the rather complex synthetic protocols used to synthesize many of these previous catalysts, the Nafion-modified Cu catalyst reported here is produced using a simple dropcasting protocol. Due to the high NH_3 Faradaic efficiency using 6 μm of Nafion, we used this Nafion thickness for all subsequent experiments. We also investigated dropcasting a mixture of polyvinylidene fluoride (PVDF) and Nafion onto the Cu electrodes. PVDF is a hydrophobic polymer that is impermeable to protons, and if used in a pure form as a catalyst overlayer, PVDF completely inhibits electrocatalysis.[30] For this reason, we used mixtures of PVDF and Nafion to explore the effect of the resulting catalysts that contain more hydrophobic fluoropolymer overlayers. With a Cu electrode at -1.4 V with an overlayer consisting of 10 wt. % PVDF in Nafion, the Faradaic efficiencies for NH_3 and NO_2^- are (41 ± 1)

% and (26.6 ± 0.1) %, respectively. The same system with a 50 wt. % PVDF in Nafion overlayer yields NH_3 and NO_2^- with Faradaic efficiencies of (22 ± 3) % and (18 ± 4) %, respectively. These results demonstrate that increasing the hydrophobicity of the fluoropolymer overlayer does not increase NH_3 Faradaic efficiency.

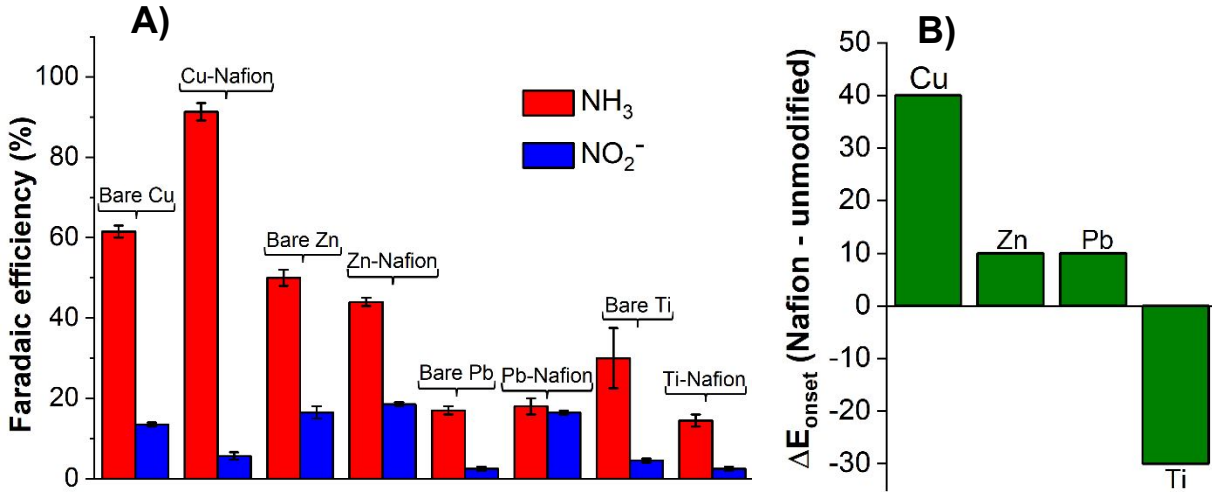

Figure 2: Faradaic efficiencies of NH_3 (A, red bars) and NO_2^- (A, blue bars) production after 1 hour of chronoamperometry from unmodified (bare) and metal electrodes modified with 6 μm of Nafion. Differences in onset potentials (ΔE_{onset}) of LSVs of NO_3^- reduction between Nafion-modified and unmodified electrodes (B).

To understand how the Nafion layer, in the absence of PVDF, improves the selectivity of Cu for NH_3 production, we first determined the interface at which NO_3^- reduction occurs on Nafion-modified electrodes. In principle, NO_3^- reduction could occur at the polymer-electrolyte interface, the electrode-polymer interface, or the electrode-electrolyte interface. The uniform nature of the Nafion overlayer (Figure S1) suggests that NO_3^- reduction does not occur at the electrode-electrolyte interface. Experiments with Nafion-modified metals other than Cu demonstrate that the product distributions vary depending upon the identity of the metal (Figure 2). These results indicate that NO_3^- reduction does not occur at the polymer-electrolyte interface because in this case, we would expect to obtain similar Faradaic efficiencies regardless of the metal

buried below the polymer. As a result, we conclude that NO_3^- reduction occurs at the electrode-polymer interface.

Unlike Cu, Nafion-modified Zn and Pb electrodes do not exhibit significantly altered NH_3 Faradaic efficiencies relative to their unmodified metal counterparts (Figures 2, S11, and S12). The electrochemical behavior of Nafion-modified Zn and Pb electrodes also differ from Nafion-modified Cu in that the LSV onset potentials of the membrane-modified electrodes do not change significantly compared to those of the corresponding unmodified metals (Figures S13 and S14). Furthermore, a Nafion-modified Ti electrode generates a lower yield of NH_3 compared to unmodified Ti (Figures 2 and S15). In the case of the Ti LSVs, the LSV for the Nafion-modified electrolyte possesses a significantly more negative onset potential than the LSV of unmodified Ti (Figure S16). Comparing the LSV and NH_3 yield results across the four metal electrodes reveals a conspicuous trend. There is a correlation between the differences in onset potentials (ΔE_{onset}) and the differences in NH_3 Faradaic efficiencies (ΔFE_{NH_3}) between the Nafion-modified and unmodified electrodes (Figure 2B). In particular, the ΔE_{onset} (+40 mV) and ΔFE_{NH_3} (+30%) values for Cu are both much greater than zero, the ΔE_{onset} (+10 mV) and ΔFE_{NH_3} (-6% for Zn and 0% for Pb) values for Zn and Pb are both near zero, and the ΔE_{onset} (-30 mV) and ΔFE_{NH_3} (-15%) for Ti are both much less than zero. This simple relationship could be used as a guide for future experimental and computational work striving to design new NO_3^- reduction catalysts that selectively produce NH_3.

Mechanistic Studies of NO_3^- Reduction on Nafion-modified Electrodes

To further understand the origin of the significant increase in NH_3 selectivity upon Nafion modification of the Cu electrode, we performed a series of experiments aimed at probing the mechanisms of NO_3^- reduction on Nafion-modified and unmodified Cu. Previous literature

indicates that NH_3 production from NO_3^- on Cu occurs via the successive production of metal-bound NO_2^- and NO intermediates.[47] As with NO_3^- reduction, we find that NO_2^- reduction at the same concentration of electrolyte (50 mM) on Cu results in a greater Faradaic efficiency in the presence of the Nafion layer (Figure 3, middle two bars, and Figure S17). Similarly, NO reduction from a NO-saturated Na_2SO_4 electrolyte on the Nafion-modified Cu electrode produces NH_3 with greater selectivity than on unmodified Cu (Figure 3, rightmost two bars, and Figure S18). These results suggest that the Nafion-induced increase in NH_3 selectivity observed for NO_3^- reduction is due, at least in part, to an increase in the kinetics of NO conversion to NH_3. This interpretation that NO reactivity on Cu is activated by Nafion is further supported by DFT calculations (*vide infra*).

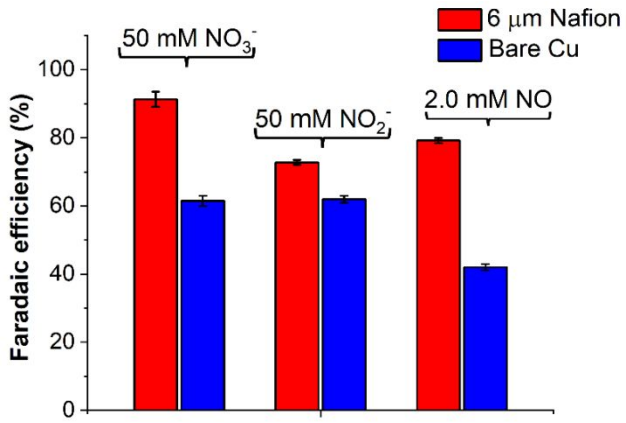

Figure 3: Comparison of Faradaic efficiencies for NH_3 production from NO_3^- reduction (leftmost two bars), NO_2^- reduction (middle two bars), and NO reduction (rightmost two bars) using Cu electrodes modified with 6 μm of Nafion (red bars) and unmodified Cu electrodes (blue bars) after 1 hour of chronoamperometry at -1.4 V. The solutions used contain 100 mM Na_2SO_4 as a supporting electrolyte.

Although the Faradaic efficiencies for NH_3 are all greater with Nafion as compared to unmodified Cu for NO_3^-, NO_2^-, and NO reduction, there is variation in the NH_3 yields for the Nafion-modified electrodes across the three electrolytes (Figure 3, red bars). In particular, the Nafion-modified electrode possess a lower selectivity for NH_3 during NO_2^- reduction, (72.8 ± 0.7) %, compared to NO_3^- reduction, (91 ± 2) %. When a Nafion-modified Cu electrode in an electrolyte containing 25 mM $NaNO_3$ and 25 mM $NaNO_2$ is used, the Faradaic efficiency for NH_3, (71 ± 1)

%, is the same within experimental error as when the electrolyte contains 50 mM $NaNO_2$, (72.8 ± 0.7) %. These results indicate that NO_3^- reduction to NH_3 is inhibited in the presence of NO_2^-, which is consistent with previous findings for other Cu-based catalysts that show NH_3 production can be affected by bulk NO_2^-.[41] Furthermore, the Nafion-modified Cu electrode also exhibits decreased NH_3 selectivity for NO reduction as compared to NO_3^- reduction due to the lower concentration of NO in a NO-saturated electrolyte (2 mM) compared to the NO_3^- electrolyte (50 mM). Indeed, both NO_3^- and NO_2^- reduction on unmodified Cu electrodes with lower concentration electrolytes (i.e. 2 mM NO_3^- or 2 mM NO_2^-) result in significantly diminished NH_3 yields, (13 ± 1) % and (11 ± 1) %, for NO_3^- and NO_2^-, respectively.

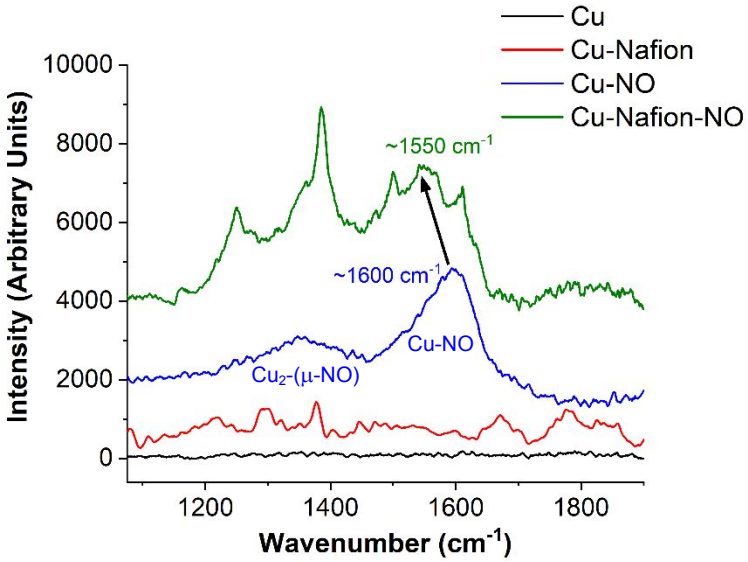

Figure 4: Surface-enhanced Raman spectra of an unmodified Cu electrode (black line), a Nafion-modified Cu electrode (red line), a Cu electrode exposed to NO (blue line), and a Nafion-modified Cu electrode exposed to NO (green line) at open circuit potential.

To further investigate the mechanism of NO_3^- reduction on Nafion-modified Cu, we used surface-enhanced Raman spectroscopy (Figure 4). First, we collected the Raman spectrum of an unmodified Cu substrate, which does not contain any peaks (Figure 4, black line). After NO was sparged across the Cu surface, the spectrum possesses two broad peaks centered around 1600 cm^{-1} and 1350 cm^{-1} (Figure 4, blue line). The more intense peak at 1600 cm^{-1} is assigned to a NO

stretching mode in Cu-NO, the frequency of which is similar to previously reported metal-nitrosyl complexes.[48] The broader peak centered around 1350 cm^{-1} is assigned to NO stretching in bridging species with multiple Cu sites such as Cu_2-(μ-NO). As is the case here, the vibrational modes of analogous bridging metal-NO and metal-CO species have significantly lower wavenumbers than their unbridged counterparts.[49,50] The relative broadness of both peaks is likely due to the presence of multiple NO binding modes and crystal faces of the polycrystalline Cu substrates.

The Raman spectrum of a Nafion-modified Cu substrate possesses a series of weak, but relatively sharp peaks from 1200 cm^{-1} to 1800 cm^{-1} due to various vibrational modes arising from Nafion. After NO was sparged across the Nafion-modified Cu surface, sharp peaks corresponding to Nafion are still observed, however, the broad NO peak at 1600 cm^{-1} on unmodified Cu shifts to 1550 cm^{-1} in the presence of Nafion. This decrease in the frequency of NO stretching on the Nafion-modified electrode indicates that the NO bond is weakened when it is covered by the polymer. This weaker NO bond explains why a Nafion overlayer increases NH_3 selectivity on a Cu electrode. In other words, the Nafion layer activates the NO bond, which increases the kinetics of NH_3 formation. Next, we use DFT calculations to further understand the reactivity of NO inside Nafion-modified Cu and to corroborate the Raman spectroscopy results.

DFT Calculations

Periodic DFT PBE-D3 calculations were performed on a 4×4 slab of Cu(111) with three layers while holding atoms in the bottom layer fixed.[51,52] Spurious interactions of images were prevented by using a length of 50 Å in the direction perpendicular to the slab surface. Nafion was modeled with $[CF_3O(CF_2)_2SO_3]^-[H_3O]^+(H_2O)_2$; ergo an hydronium and two explicit water molecules are associated with the sulfonate group. Without Nafion, we considered absorption with a water trimer (Figure 5A). In both cases, there are hydrogen-bonding interactions between explicit

water molecules and NO. The N-O bond distance is 1.247 Å on Cu(111), becoming slightly elongated to 1.252 Å when NO interacts with explicit water molecules associated with the sulfonate and hydronium of Nafion. The Nafion also causes NO to be more closely bound to the surface, 1.227 Å, versus 1.235 Å. These structural differences lead to lowered wavenumbers for the N-O vibrational stretching mode in the presence of Nafion (Figure 5). Indeed, the calculated difference in these stretching frequencies, $\Delta\upsilon$ = 45 cm^{-1}, between the Nafion-modified and unmodified Cu(111) surfaces agrees well with the experimental Raman data ($\Delta\upsilon \sim 50$ cm^{-1}, Figure 4), although the absolute values of the calculated harmonic frequencies underestimate the values measured experimentally. This underestimation is expected and has been observed previously for vibrational calculations using the PBE-D3 functional.[53]

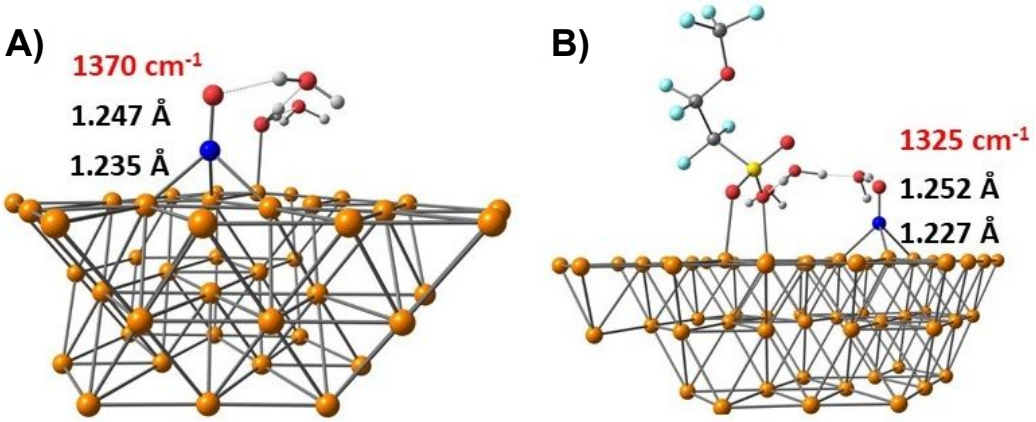

Figure 5: Structural properties of NO adsorbed at the Cu(111) surface with (A) water and (B) a model for Nafion, an associated hydronium, and water molecules.

The reaction path for the NO → NH_3 process was calculated on Cu(111) and Nafion-coated Cu(111) (Figure 6). We used a hydronium ion solvated by three water molecules and an excess electron, [H_9O_4], as the source of protons and electrons; following the recommendations of Rossmeisl et al.[54] We then added an additional H atom after each reduction step. In the presence of Nafion, reaction energies of the *NO → *NOH, *NOH → *N + H_2O, *N → *NH, *NH → *NH_2, and *NH_2 → *NH_3 steps are all lowered. Interestingly, the greatest impact is found for the

first hydrogenation step, the potential-limiting step, indicating that Nafion and the water around its associated proton sufficiently perturb surface-adsorbed NO to affect energetics of NO reduction to NH_3.[55] Analogous computations on Zn(001) and Nafion-coated Zn(001) surfaces provide *NO → *NOH reaction energies of -0.90 eV and -1.02 eV, respectively. Thus for Zn(001), Nafion has an impact of -0.13 eV, a factor of 4.1 smaller than the impact on Cu(111) (Figure 6), which agrees with our experimental data indicating that a Nafion-modified Zn electrode does not display a significantly altered NO_3^- reduction product distribution as compared to unmodified Zn (Figure 2). Taken together, these results demonstrate that it is the activation of the NO bond by Nafion that enables the Nafion-modified Cu electrode to display enhanced selectivity for NH_3 production.

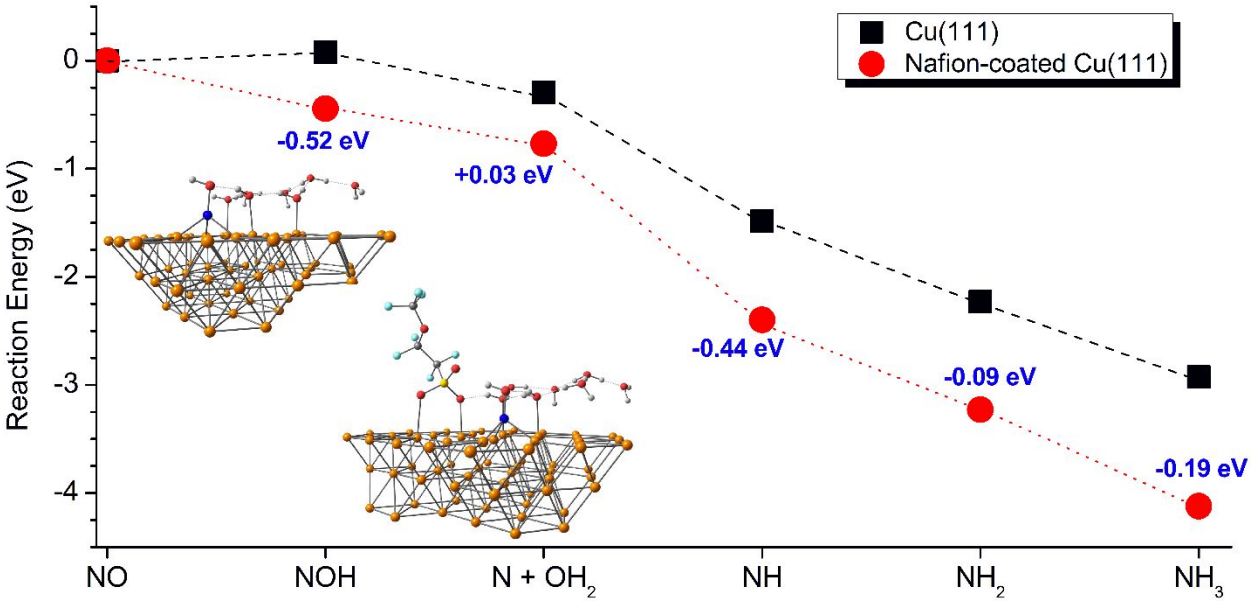

Figure 6: Calculated reaction path for NO reduction to NH_3 on Cu(111) and Nafion-coated Cu(111) obtained from DFT. The impact of Nafion on reaction energies are given in blue and insets show optimized structures of the *NOH species.

Denitrification of Groundwater

Lastly, we tested the practicality of the Nafion-modified Cu electrode by using it to remove NO_3^- from a real-world groundwater sample. We obtained groundwater from a rural residential well in Silver Springs, Nevada, which is located in an agricultural valley 30 miles east of Reno,

Nevada. Groundwater NO_3^- contamination is common in regions like these due to agricultural runoff from fertilizers. The NO_3^- concentration measured in the well water was 0.24 ppm, which is more than double the 0.10 ppm average for commercially treated water in Reno.[56] We used the Nafion-modified Cu electrode to denitrify the well water directly without the addition of a supporting electrolyte. After one hour of chronoamperometry at -1.4 V vs. Ag/AgCl, the NO_3^- concentration in the water decreased from 0.24 ppm to 0.008 ppm, which represents a 97% NO_3^- removal efficiency (Figure S19). These results demonstrate that the Nafion-modified Cu catalyst has potential for practical use in water purification.

Conclusions

In summary, this work discusses electrochemical NO_3^- reduction to NH_3 using simple Nafion-modified metal catalysts. For the case of Nafion-modified Cu, which produces NH_3 with excellent selectivity, the Nafion overlayer activates the NO bound in a Cu-NO intermediate, which accelerates NH_3 generation. This interpretation is supported by surface-enhanced Raman spectroscopy data and DFT calculations. In addition to demonstrating the practical applicability of these catalysts for water purification, this work opens up a new research direction for the development of selective NO_3^- reduction catalysts using membrane-modified electrodes.

Author Contributions

All authors designed the experiments, discussed the results, and commented on the manuscript. P.M. and A.J.A.A. performed the experiments. P.M. and C.J.B. analyzed the data. P.M., C.J.B., and S.O.O. wrote the paper. D.P. performed DFT calculations. C.J.B. conceived the project.

Competing Interest

The authors declare no competing interests.

Acknowledgements

C.J.B., P.M., and A.J.A.A. acknowledge that this material is based upon work supported by the National Science Foundation CAREER Award under Grant No. CHE2046105. S.O.O. and D.P. were supported by the National Science Foundation under Grant No. 18003887. The authors acknowledge the Shared Instrumentation Laboratory in the Department of Chemistry at UNR. SEM-EDS analysis was done in the Mackay Microbeam Laboratory at UNR, and the authors thank J. Desormeau for his kind assistance. The National Science Foundation (CHE-1429768) is acknowledged for the X-ray diffractometer.

References

1. S. L. Foster, S. I. P. Bakovic, R. D. Duda, S. Maheshwari, R. D. Milton, S. D. Minteer, M. J. Janik, J. N. Renner and L. F. Greenlee, *Nat. Catal.,* 2018, **1**, 490–500.
2. C. Tang and S. Z. Qiao, *Chem Soc Rev.,* 2019, **48**, 3166–3180.
3. R. F. Service, *Science,* 2014, **345**, 610-610.
4. Y. Ashida, K. Arashiba, K. Nakajima and Y. Nishibayashi, *Nature*, 2019, **568**, 536–540.
5. A. Bhown and E. Cussler, *J. Am. Chem. Soc.,* 1991, **113**, 742–749.
6. F. Jiao and B. Xu, *Adv. Mater*., **2019,** *31,* 1805173.
7. A. Afif, N. Radenahmad, Q. Cheok, S. Shams, J. H. Kim and A. K. Azad, *Renew. Sustain. Energy Rev,* 2016, **60**, 822–835.
8. G. Ertl and *J. Vac. Sci. Technol. Vac. Surf. Films,* 1983, **1**, 1247–1253.
9. V. Kyriakou, I. Garagounis, E. Vasileiou, A. Vourros and M. Stoukides, *Catal. Today.,* 2017, **286**, 2–13.
10. T. Wu, W. Fan, Y. Zhang and F. Zhang, *Mater. Today Phys.,* 2021, **16**, 100310–100332.

11. V. Kyriakou, I. Garagounis, A. Vourros, E. Vasileiou and Stoukides, *Joule,* 2020, **4***,* 142–158.

12. Y. Wan, J. Xu and R. Lv, *Mater. Today.,* 2019, **27***,* 69–90.

13. B. H. Suryanto, H. L. Du, D. Wang, J. Chen, A. N. Simonov and D. R. MacFarlane, *Nat. Catal.,* 2019, **2***,* 290–296.

14. C. Guo, J. Ran, A. Vasileff and S. Z. Qiao, *Energy Environ. Sci,* 2018, **1***,* 45–56.

15. C. F. Chen, X. Cao, S. Wu, X. Zeng, L. X. Ding, M. Zhu and H. Wang, *J. Am. Chem. Soc.,* 2017, **139***,* 9771–9774.

16. A. Stirling, I. Pápai, J. Mink and D. R. Salahub, *J. Chem. Phys.,* 1994, **100***,* 2910–2923.

17. A. Menció, J. Mas-Pla, N. Otero, O. Regàs, M. Boy-Roura, R. Puig, J. Bach, C. Domènech, M. Zamorano and D. Brusi, *Sci. Total Environ.* 2016, **539***,* 241–251.

18. S. Garcia-Segura, M. Lanzarini-Lopes, K. Hristovski, P. Westerhoff, *Appl. Catal. B Environ.* 2018, **236***,* 546–568.

19. M. H. Ward, R. R. Jones, J. D. Brender, T. M. De Kok, P. J. Weyer, B. T. Nolan, C. M. Villanueva and S. G. Van Breda, *Int. J. Environ. Res. Public. Health,* 2018, **15**, 15-45.

20. J. R. Self and R. Waskom, *Colorado State University* Fact Sheet, No 1992, **0517***,* 1–3.

21. B. Kross, *J Prev Med,* 2002, **10***,* 3–10.

22. J. Martínez, A. Ortiz, I. Ortiz, *Appl. Catal. B Environ.,* **2017,** 207, 42–59.

23. G. E. Dima, A. C. A. de Vooys and M. T. M. Koper, *J. Electroanal. Chem. Lausanne Switz.,* 2003, **554–555***,* 15–23.

24. I. Katsounaros and G. Kyriacou, *Electrochimica Acta,* 2008, **53***,* 5477–5484.

25. S. Pronkin, P. Simonov, V. Zaikovskii and E. Savinova, *J. Mol. Catal. Chem.,* 2007, **265***,* 141–147.

26. K. Shimazu, R. Goto, S. Piao, R. Kayama, K. Nakata and Y. Yoshinaga, *J. Electroanal. Chem.,* 2007, **601***,* 161–168.

27. S. Piao, Y. Kayama, Y. Nakano, K. Nakata, Y. Yoshinaga and K. Shimazu, *J. Electroanal. Chem.* 2009, **629***,* 110–116.

28. E. Pérez-Gallent, M. C. Figueiredo, I. Katsounaros and M. T. M. Koper, *Electrochimica Acta,* 2017, **227***,* 77–84.

29. S. N. Supakul and C. J. Barile, *Front. Chem.,* 2018, **6***,* 1-8.

30. H. Pan and C. J. Barile, *Energy Environ. Sci.,* 2020, **13**, 3567–3578.

31. F. Lei, W. Xu, J. Yu, K. Li, J. Xie, P. Hao, G. Cui and B. Tang, *Chem. Eng. J.,* 2021, **426***,* 131317–131323.

32. I. Katsounaros, M. Dortsiou, C. Polatides, S. Preston, T. Kypraios and G. Kyriacou, *Electrochimica Acta,* 2012, **71***,* 270–276.

33. Y. Hori, K. Kikuchi and S. Suzuki, *Chem. Lett.,* 1985, **14***,* 1695–1698.

34. R. Kortlever, J. Shen, K. J. P. Schouten, F. Calle-Vallejo and M. T. M. Koper, *J. Phys. Chem. Lett.,* 2015, **6***,* 4073–4082.

35. M. A. Hasnat, I. Ishibashi, K. Sato, R. Agui, T. Yamaguchi, K. Ikeue and M. Machida, *Bull. Chem. Soc. Jpn.,* 2008, **81***,* 1675–1680.

36. M. Machida, K. Sato, I. Ishibashi, M. A. Hasnat and K. Ikeue, *Chem. Commun.,* 2006, **7***,* 732–734.

37. G. Brauer, Inorganic chemistry: Vol. 1. Reed F. Riley, Ed. Academic Press, New York, NY 1963.

38. I. G. Zacharia and W. M. Deen, *Ann. Biomed. Eng.,* 2005, **33***,* 214–222.

39. C. Polatides and G. Kyriacou, *J. Appl. Electrochem.,* 2005, **35***,* 421–427.

40. N. H. Furman, 1939, "Scott's Standard Methods of Chemical Analysis," 5th ed. D. Van Nostrand and Co., New York, NY, pg. 630.

41. G. F. Chen, Y. Yuan, H. Jiang, S. Y. Ren, L. X. Ding, L. Ma, T. Wu, J. Lu and H. Wang, *Nat. Energy,* 2020, **5***,* 605–613.

42. B. Schnetger and C. Lehners, *Mar. Chem.,* 2014, **160***,* 91–98.

43. G.W. Watt and J. D. Chrisp, *Anal. Chem.* 1952, **24***,* 2006–2008.

44. H. Liu, J. Park, Y. Chen, Y. Qiu, Y. Cheng, K. Srivastava, S. Gu, B. H. Shanks, L. T. Roling and W. Li, *ACS Catal.,* 2021, **11***,* 8431–8442.

45. D. P. Butcher Jr. and A. A. Gewirth, *Nano Energ.,* 2016, **29**, 457–465.

46. M. Yamauchi, R. Abe, T. Tsukuda, K. Kato and M. Takata, *J. Am. Chem. Soc.,* 2011, **133***,* 1150–1152.

47. Z. Y. Wu, M. Karamad, X. Yong, Q. Huang, D. A. Cullen, P. Zhu, C. Xia, Q. Xiao, M. Shakouri, F. Y. Chen, J. Y. (Timothy) Kim, Y. Xia, K. Heck, Y. Hu, M. S. Wong, Q. Li, I. Gates, S. Siahrostami and H. Wang, *Nat. Commun.,* 2021, **12**, 2870–2879.

48. J. E. Huheey, E. A. Keiter and R. L. Keiter, 4th Ed. *Pearson College Division*, New York, NY 1993.

49. C. De La Cruz and N. Sheppard, *Spectrochim. Acta. A. Mol. Biomol. Spectrosc.,* 2011, **78***,* 7–28.

50. K. G. Schmitt and A. A. Gewirth, *J. Phys. Chem., C,* 2014, **118***,* 17567–17576.

51. J. P. Perdew, K. Burke and M Ernzerhof, *Phys Rev Lett.,* 1996, **77***,* 3865–3868.

52. S. Grimme, J. Antony, S. Ehrlich and H. Krieg, *J. Chem. Phys.,* 2010, **132***,* 154104.

53. I. M. Alecu, J. Zheng, Y. Zhao and D. G. Truhlar, *J. Chem. Theory Comput.,* 2010, **6***,* 2872–2887.

54. J. Rossmeisl, E. Skúlason, M. E. Björketun, V. Tripkovic and J. K. Nørskov, *Chem. Phys. Lett.,* 2008, **466***,* 68–71.

55. H. Wan, A. Bagger and J. Rossmeisl, *Angew. Chem.,* 2021, **133***,* 22137–22143.

56. M. Foree, 2021 Water quality report. *Truckee Meadows Water Authority,* 2021, 1–5.